Journal of Optoelectronics and Advanced Materials Vol. 2, No. 1, March 2000, p. 13-30

REVIEW PAPER

WHAT CAN WE LEARN FROM HIGH PRESSURE STUDIES?

Hans D. Hochheimer

Department of Physics, Colorado State University, Fort Collins, CO 80523, USA

Several methods used in combination with high pressure to study phase transitions are described. The usefulness of these methods is then demonstrated by presenting results of a number of studies of materials which undergo structural phase transitions or isostructural transitions, where the valence state of the atom or the nature of the spin-density wave state changes with pressure.

(Received January 27, 2000; accepted after revision March 15, 2000)

Keywords: Phase transitions, Valence transitions, Raman scattering, Brillouin scattering, Energy dispersive X-ray diffraction, Conductivity measurements

1. Introduction

The interest in high pressure studies, not only in physics and chemistry, has increased with a rapid pace. It is very well documented in the Proceedings of the International Conference-AIRAPT - 16 and HPCJ-38- on High Pressure Science and Technology, Kyoto, Japan [1]. One of the reasons for this development is due to the fact that the progress of the diamond anvil cell (DAC) has made pressure studies easier and less cost intensive, and at the same time has extended the pressure of the studies in the Megabar range. The motivation to achieve higher and higher pressures was driven by the search for metallization of hydrogen and other insulating or semiconducting materials under pressure. In this paper it is demonstrated that studies in the pressure range up 200 kbar (20 GPa) are very useful and can provide new insights and a deeper understanding of the underlying physics. It is well known that most physical properties depend on the lattice constants, and pressure studies can shed light on this dependence. Even more interesting and more important is the fact that in many materials a delicate balance of interactions determines in which structure the material crystallizes. Minor changes in this balance will lead to a phase transition, and the pressure dependence of this transition temperature will provide information about these interactions and their importance for the stabilization of a certain structure. In addition, pressure is a very "clean" parameter compared with temperature. Of course, if one lowers the temperature one also decreases the lattice constant as in the case of increasing pressure. But, contrary to pressure, temperature changes also the anharmonicities [2,3] in the solid and effects of the change of the lattice constant cannot be separated from effects due to changes in the anharmonicities. In fact, measurements of the pressure dependence at constant pressure and measurements of the temperature dependence at constant pressure allow to determine the anharmonic contributions [4,5]. The purpose of this paper is to provide a review of the most common methods used for studying the effects of pressure and give some examples, where pressure studies have led to a deeper understanding of the physics involved by changing the lattice constants or extending the studies to a wider range of the p-T-phase diagram.

2. Methods

Raman scattering and energy dispersive X-ray diffraction are the most widely used methods to study pressure induced phase transitions. There are many publications describing the theory and application of the Raman effect [6,7]. Each elementary Raman scattering event involves three basic processes: 1) the destruction of a photon of frequency Ti, incident from the light source, 2) the creation (Stokes) or annihilation (Anti Stokes) of a phonon of frequency Tph, and 3) the creation of a scattered photon of frequency ω_s. If one treats this three step scattering process by third order perturbation theory one obtains the well known form for the Raman tensor with an energy denominator [6] which gives rise to resonant Raman scattering in case that the energy of the incident light approaches the energy of the band gap of the crystal. The nearly forgotten semi-classical derivation by Born and Bradbury [8] provides, however, a deep insight in the physics involved in the Raman scattering process.

The basic ideas of this semi-classical calculation are the following:

1. The electric vector Re{ $\vec{E}$ exp (-iωt)} of the incident light beam produces an electric moment, $\vec{M}$ in the crystal. $\vec{M}$ is given by

$$M_i = \sum_j \alpha_{ij} E_j \tag{1}$$

with α_{ij}, the polarizability tensor associated with the electrons in the crystal.

2. The scattered light is produced by re-radiation of energy by the oscillating dipole moment, $\vec{M}$.

$$I_s \sim \frac{1}{\lambda^4}\left|\vec{M}\right|^2 \tag{2}$$

3. Due to the electron-lattice interaction, the electronic eigenvalues and wave functions in a diatomic lattice depend on the lattice displacement amplitude, $\vec{r}$, of the sublattices, and the electronic polarizability can be expanded in a power series in $\vec{r}$:

$$\alpha_{ij} = \alpha_{ij}^{(0)} + \sum_k \alpha_{ij,k} r_k + \sum_{k,l} \alpha_{ij,kl} r_k r_l + O(r^3) + \ldots \tag{3}$$

where $\alpha_{ij}^{(0)}$ determines the intensity of the elastically scattered light (Rayleigh scattering), and $\alpha_{ij,k} = \left(\frac{\partial \alpha_{ij}}{\partial \alpha_k}\right)_{r=0}$ and $\alpha_{ij,kl} = \left(\frac{\partial^2 \alpha_{kl}}{\partial r_k \partial r_l}\right)_{r=0}$ give rise to first and second order Raman scattering, respectively.

As

$$\alpha \sim e^{-i\omega_0 t} \text{ and } \vec{r} \sim e^{\mp i\omega_{ph} t}$$

we expect

$$\vec{E}_s \sim e^{-(\omega_0 \pm \omega_{ph})t} \tag{4}$$

with ω_0 and ω_{ph} the laser frequency and frequency of the phonon, respectively.

If we compare the wavenumber of the incident light with the typical maximum value of the phonon wave vector, we see that we can only see phonons from the center of the Brillouin zone with first order Raman scattering. The typical maximum value of a phonon wave vector is about 3×10^8 cm^{-1}. Incident light with a wavenumber of 20,000 cm^{-1} (λ = 500 nm) has a wave vector inside the crystal of the order 2×10^5 cm^{-1}. Assuming 90° scattering we have then

$$k = 2k_i \sin\frac{\theta}{2} = \sqrt{2} \times 2 \times 10^5 \text{ cm}^{-1} \tag{5}$$

This value is small compared with the maximum value of the phonon wave vector. Therefore we can observe only phonons from the center of the Brillouin zone with first order Raman effect, or in other words, phonons of importance in the first order Raman effect have wavelengths very long compared with the lattice constants.

The Raman scattering apparatus consisting basically of a laser, imaging optics, and a monochromator with photon counting system (photomultiplier, high voltage supply, and counting electronics) can also be used to measure luminescence spectra. Luminescence spectra can be distinguished easily from Raman spectra, since their peak positions does not depend on the frequency of the exciting laser light. Replacing the laser by a high pressure Xenon or halogen lamp allows then also the measurements of absorption spectra with the same equipment.

Energy dispersive X-ray diffraction has been described in detail by Will [9], Bordas et al. [10], and Buras et al. [11]. In Fig 1. the experimental set-up for energy dispersive X-ray diffraction is shown. It is quite clear that this technique is advantageous in combination with diamond anvil cells. The diamond anvil cell limits the range of angles of the diffracted X-ray beams. Measurements at a fixed angle allow to take care of this problem. Compared with angle dispersive X-ray diffraction, energy dispersive X-ray diffraction has a worse resolution, i.e. the error in the lattice constant is of the order 10^{-3} compared with 10^{-5} with angle dispersive X-ray diffraction. In order to see that, we write the Bragg equation $2\, d_{hkl} \sin\theta = \lambda_R$ using $\lambda_R = hc/ER$ with λ_R in [Å] and ER in [keV] as.

$$E_R d_{hkl} \sin\theta_0 = 6.1990525 \text{ keVÅ} \tag{6}$$

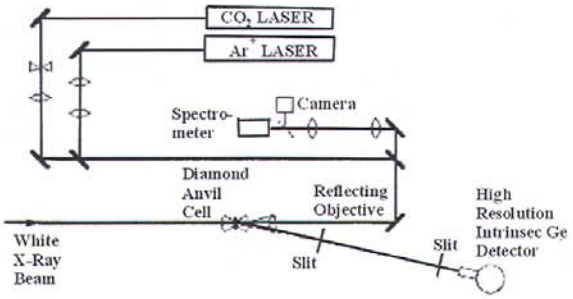

Fig. 1. Schematic diagram of the experimental setup for energy dispersive X-ray diffraction at high pressures.

Here E_R is the energy which belongs to the reflection with the Miller indices hkl, or in other words from X-rays diffracted from planes (hkl) with a spacing d_{hkl}.
In Fig. 2 the energies for the reflection hkl are shown as a function of the angle 2θ(°).

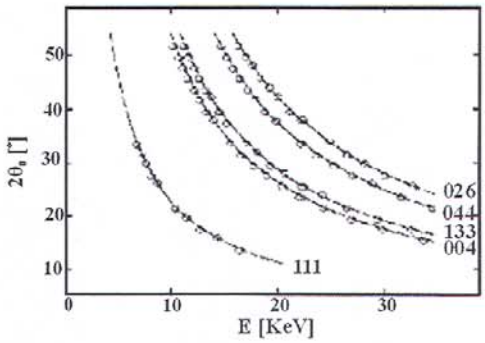

Fig. 2. Peak positions of some reflections hkl of silicon powder. The circles represent experimental points and the full lines are theoretical curves (Data taken from ref. 11).

Another advantage of the technique is seen from the Fig. 2. Since the energy position of a reflection depends on the angle one can easily move reflections which may be masked by fluorescence into a energy position where they are not masked anymore, because contrary to the reflections, fluorescence lines do not move, if the angle is changed. In the case that the angular error and the error in the energy determination are uncorrelated, the error, D_R, for a special reflection hkl is given by:

$$D_R = \left[\left(D_R^\theta\right)^2 + \left(D_R^E\right)^2\right]^{1/2} \tag{7}$$

with $D_H^\theta = \left| -\frac{E_R ctg\theta_o \Delta\theta_o}{E_H} \right| = ctg\theta_o \Delta\theta_o$ and, D_R^E, the errors due to the error in the angle determination (Fig. 3) and energy resolution of the detector (Fig. 4), respectively.

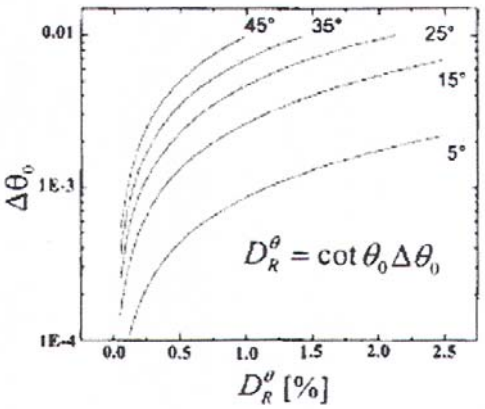

Fig. 3. Error due to divergence $\Delta\theta_o$ for various scattering angles (Data taken from ref. 11).

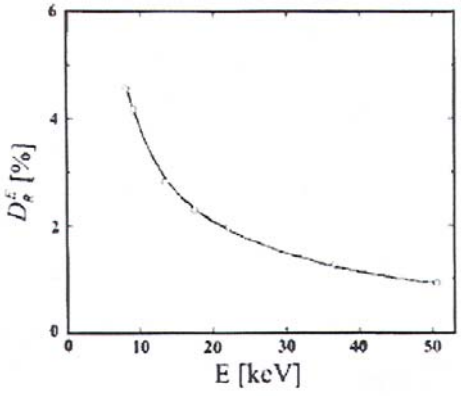

Fig. 4. Error due to the energy resolution of the detector determined experimentally from the widths of X-ray fluorescence peaks. (Data taken from ref. 11).

The energy resolution favours according to eq. 6 small scattering angles and small interplanar spacing, i.e. high index reflections.

Brillouin scattering, the scattering of light by acoustic phonons, however, has not been used intensively to study pressure induced phase transitions. This is due to the fact, that the single crystal is destroyed when a structural phase transition occurs. For the analysis of the Brillouin data, however, the knowledge of the crystal orientation is crucial. Nevertheless, it has been proven that high pressure Brillouin studies are quite useful [12-18].

As shown in Fig. 5a the very strong quasi elastic Rayleigh scattering in solids due to imperfections in the crystal causes problems in resolving the Brillouin peaks. In liquids the ratio of the intensity Rayleigh peak (elastically scattered light) and the intensity of the Brillouin peaks is given by the Landau-Placzek relation

$$\frac{I_R}{2I_B} = \frac{c_p - c_v}{c_v} = \gamma - 1 \approx 1 \tag{8}$$

In solids the ratio of the intensity of the quasi Rayleigh scattering and the intensity of the Brillouin peaks is of the order 10^4 - 10^5.

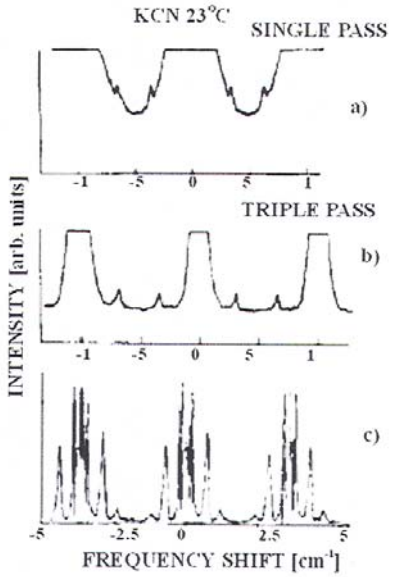

Fig. 5. Intensity ratios of the Rayleigh and Brillouin peaks a) single pass; b) triple pass; c) triple pass with smaller free spectral range and higher finesse of the Fabry-Pérot interferometer.

One can, however, increase the contrast factor of a Fabry-Pérot interferometer by using a multipass arrangement, i.e. one reflects the scattered light beam and sends it several times through the interferometer. It was the pioneering work of Sandercock [19-21] that allowed the wide spread use of such multipass Fabry-Pérot interferometers and led to a rapid development not only of Brillouin scattering at ambient pressure but also at high pressures. Fig. 5b shows now the Brillouin spectrum taken with a multipass Fabry-Pérot interferometer, and Fig 5c the spectrum with smaller free spectral range and a higher finesse of the interferometer. In Fig. 6 the principal arrangement for Brillouin scattering at high pressure is shown.

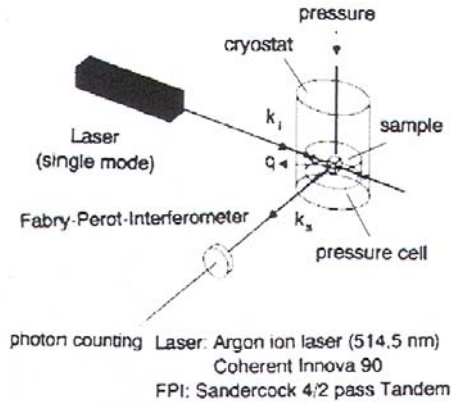

Fig. 6. Schema of a high pressure Brillouin scattering experiment.

Fig. 7 shows the high pressure cell used for these experiments. This cell can be used for pressures up to 1 GPa .

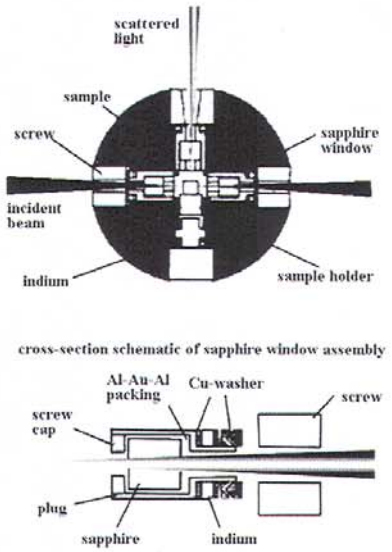

Fig. 7. Details of the high pressure cell used for Brillouin scattering.

If one wants to go to higher pressures one has to use a diamond anvil cell as described by Whitfield and Brody [22]. One can describe the scattering process as a ***Doppler*** shift experienced when incident light is ***Bragg*** reflected from a thermal phonon traveling with velocity v. The condition for ***Bragg*** reflection is:

$$\lambda_{0,n} = 2\Lambda \sin\phi \tag{9}$$

where $\lambda_{0,n}$ is the wavelength of the impinging light in the sample; Λ, the wavelength of the sound wave, and Φ, the angle between the impinging light ray and the phonon wave front. The ***Doppler*** shift is given by

$$\pm(\nu_0 - \nu) = \nu_{ph} = v/\Lambda\,;\ \nu < \nu_0 : +sign;\quad \nu > \nu_0 : -sign \tag{10}$$

With eq. (9) eq. (10) yields

$$\pm(\nu_0 - \nu) = (2v\sin\phi)\lambda_{0,n} = \{(2v\sin\phi)/c_n\}\nu_0 \tag{11}$$

where $\lambda_{0,n} = c_n/\nu_0$. Using $c_n = c_0/n$ with c_0, the speed of light in vacuum, and n, the index of refraction of the sample we finally get for the Brillouin shift $\Delta\nu$:

$$\pm(\nu_0 - \nu) = \pm\Delta\nu = 2\nu_0 v\sin\phi/c_n = (2\nu_0 vn\sin\phi)/c_0 \tag{12}$$

The fact that the index of refraction shows up in the formula for the Brillouin shift causes problems in analyzing the data at high pressure, because there are hardly any data on the pressure dependence of the index of refraction available in literature. In analyzing data up to 1 GPa one uses therefore the specific refraction to calculate the pressure dependence of the index of refraction 13,14.

In the case of Brillouin scattering at high pressure using a diamond anvil cell, Whitfield and Brody [22] came up with a very clever idea to avoid the problem with the index of refraction. By choosing the scattering geometry of Fig. 8 they were able to show that the formula for the Brillouin shift does not contain the index of refraction anymore.

Starting from eq. 10 for the Doppler shift and using $\Lambda = \lambda_{0,n}/\sin\Phi$ from eq. 9 we obtain

$$\pm(\nu_0 - \nu) = \frac{v}{\lambda_{0,n}/\sin\phi} \tag{13}$$

with

$$\lambda_{0,n} = \frac{c_n}{\nu_0} \tag{14}$$

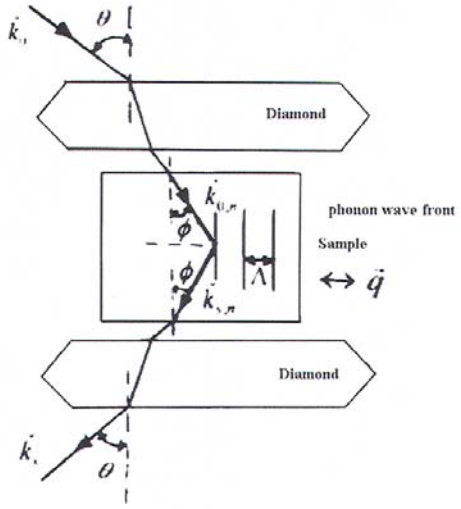

Fig. 8. Angular relationships between angle of incidence, θ, and angle Φ, in the sample.

$$\left|\vec{K}\right| = 2\pi/\lambda, \left|\vec{q}\right| = 2\pi/\Lambda$$

Substitution of eq. 14 into eq. 13 yields

$$\pm(\nu - \nu) = \frac{2\mathrm{v}\sin\phi}{\mathrm{c}_0}\nu_0 \qquad \text{or}$$

$$\pm(\nu_0 - \nu) = 2\nu_0\,\mathrm{v}\sin\phi/\mathrm{c}_n = \frac{2\nu_0\,\mathrm{v}\,\mathrm{n}\sin\phi}{c_0} \tag{15}$$

According to Snell's law we have setting the index of refraction of air equal to 1

$$n\sin\phi = \sin\theta \tag{16}$$

Substituting eq. 16 into eq. 15 yields then a formula for the Brillouin shift which does not contain the index of refraction anymore.

$$\pm(\nu_0 - \nu) = \Delta\nu = \frac{2\nu_0\,\mathrm{v}\sin\phi}{c_0} = \frac{2\mathrm{v}\sin\phi}{\lambda_0} \tag{17}$$

In Fig. 9a the scattering geometry for the Brillouin shift without the index of refraction is shown. In fact, if we change the scattering geometry now as indicated in Fig. 9b, we obtain a formula for the Brillouin shift which includes the index of refraction.

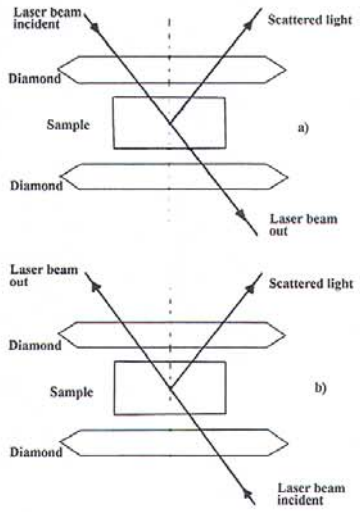

Fig. 9. Scattering geometry for Brillouin shifts a) without index of refraction b) with index of refraction in the equation for $\Delta\nu$.

By performing measurements of the Brillouin shift using both scattering geometries we can then determine the pressure dependence of the refractive index.
Fig. 10 allows us to determine the Brillouin shift connected with the scattering geometry of Fig. 9b.

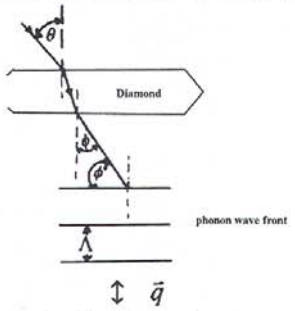

Fig. 10. Relations between angle of incidence, θ, and angles Φ and Φ' in the sample.

The wavelength of the phonon, Λ, is now given by

$$\Lambda = \frac{\lambda_{0,n}}{2\sin(90-\phi)} = \frac{\lambda_{0,n}}{2\cos\phi} \tag{18}$$

Using $\cos\phi = \sqrt{1-\sin^2\phi}$ and Snell's law $\sin\phi = \frac{\sin\theta}{n}$ we obtain

$$\frac{v}{\Lambda} = \Delta\nu = \frac{2v\sqrt{1-\sin^2\theta/n^2}}{\lambda_{0,n}} = \frac{2v\sqrt{\sin^2\theta/n^2}}{c_0}\nu_0 \tag{19}$$

Again with $\nu_0/c_0 = 1/\lambda_0$ and $c_n = c_0/n$ we obtain

$$\Delta\nu = \frac{2vn}{\lambda_0}(1-\sin^2\theta/n^2)^{\frac{1}{2}} \tag{20}$$

the Brillouin shift relevant for the scattering geometry in Fig. 9 b .

In Figs. 11 and 12 we show a schematic diagram of the Brillouin scattering apparatus and the high pressure generating systems, respectively. The conductivity measurements were done using the 4-probe technique, which eliminates the influence of contact resistance. The system is shown schematically in Fig. 13.

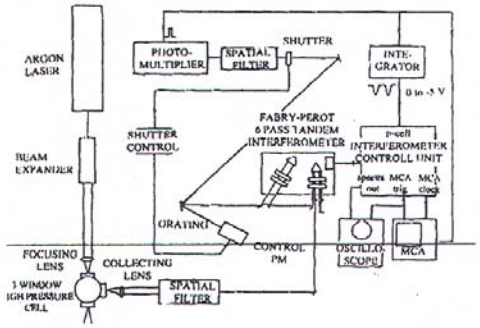

Fig. 11. Schematic diagram of the Brillouin scattering apparatus.

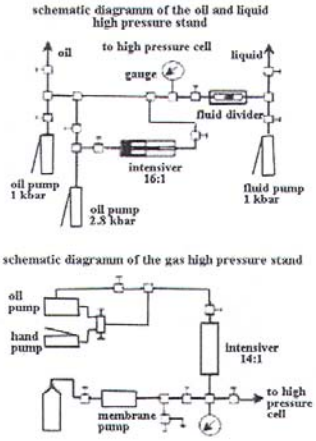

Fig. 12. Schematic diagram of the pessure generating systems using liquids (upper) and gases (lower) as pressure medium.

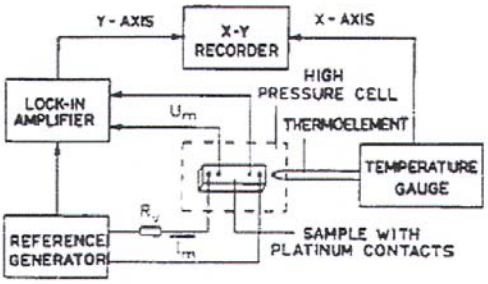

Fig. 13. Schematic diagram of the conductivity measurement system.

3. Materials

In this part results of high pressure optical studies (Raman scattering, absorption, luminescence, and Brillouin scattering measurements), of energy dispersive X-ray diffraction studies, and finally of conductivity measurements are presented. It will demonstrate the usefulness of these methods in connection with high pressure discussed in II.

3.1. Raman scattering studies

The two examples presented here show the usefulness of Raman scattering in determining the p-T phase diagram. The second example shows, however, that changes in the spectral features are not always an indication for a phase transition, but can be due to mode crossing.

a) Ammonium halides

A phase diagram of NH_4I has been determined before by piston displacement technique [23] and calorimetric measurements [24]. However, the results carry large error bars. A group theoretical analysis of the Raman spectra in the three CsCl-type phases has shown that Raman scattering can be used to determine the p-T phase diagram of the ammonium halides [25, 26]. We have done these measurements and have determined p-T phase diagrams of NH_4Br and NH_4I. In the case of NH_4I we have reduced the error bars considerably as can be seen in Fig. 14. The rectangular boxes above and below and to the right and left, respectively, of the phase lines indicate regions, where we were absolutely sure that only one phase was present. The width of the crosses indicates regions where the features of the two phases were present in the Raman spectra and can, therefore, looked upon as the size of the error bars.

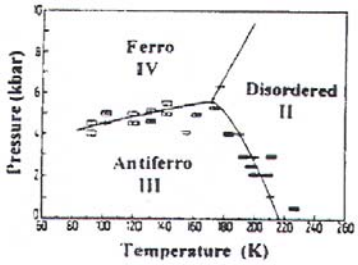

Fig. 14. Phase diagram of NH_4I.

b) Ternary chalcogenides

Though Raman scattering has been proven in the case of the ammonium halides to be a useful tool to determine phase diagrams, there is some danger to use solely Raman scattering results to determine if a phase transition has occurred. This is demonstrated in the case of the ternary chalcogenide, $TlGaS_2$. Contrary to the space group assignment, C_c [27], we have determined the space group of these materials to be $C_{2/c}$. This has allowed us to do a group theoretical analysis, which shows that there are 48 Raman-active modes with A_g and B_g symmetry, respectively. As can be seen in Fig. 15, many of the group theoretically allowed bands show up in the Raman spectra. Furthermore, it can be seen, that as well as at 300 K as at 110 K, new bands appear and old ones disappear when pressure is applied. Therefore one could conclude that a phase transition has occurred.

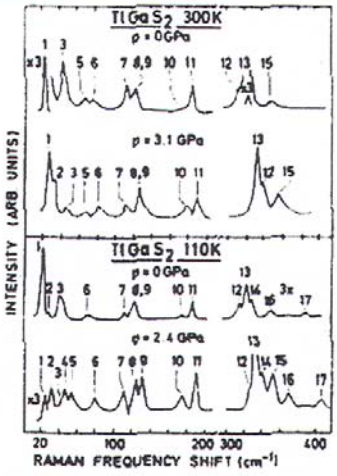

Fig. 15. Raman spectra of $TlGaS_2$ at ambient and high pressure at 300 and 110 K.

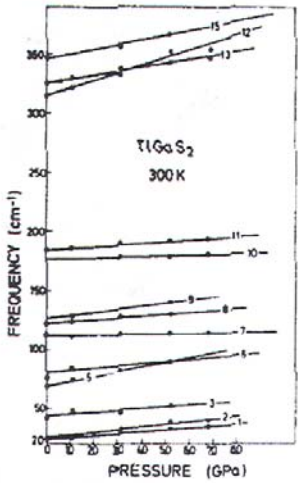

Fig. 16. Pressure dependence of the frequency mode of $TlGaS_2$.

However, one has to keep in mind that modes with different symmetry can cross each other. In fact, if one plots the pressure dependence (Fig.16) of the various modes, the crossing of modes is quite obvious and provides an explanation for the appearance and disappearance of bands in the Raman spectra other than caused by a phase transition. Figure 17 shows this mode crossing beautifully in the case of $TlInS_2$, another ternary chalcogenide with the same structure, at 110 K.

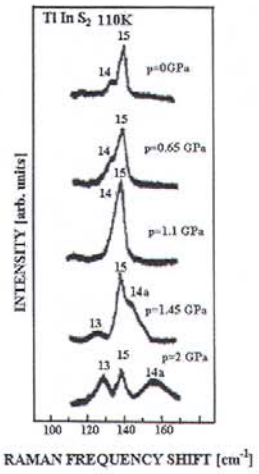

Fig.17. Raman-active bands in the frequency region between 110 and 170 cm^{-1} at various pressures at 110 K.

3. 2. Absorption measurements in copper chloride

In the late 70th quite some interest in CuCl has been generated by reports that CuCl may be a high temperature superconductor [28]. As quantitative measurements of the shift of the absorption edge with good pressure calibration were lacking, we undertook such a study. Our motivation was to see if there is any optical evidence for the insulator-metal transition, which has been reported to occur around 4 GPa [28]. Fig. 18 shows the absorption spectra in the region of stability of the zinc-blende, tetragonal, and NaCl-type phases. The absorption edge for the zinc-blende and tetragonal phases is well defined and sharp, whereas it is not for the NaCl-type phase. This indicates that in the former two phases the smallest energy gap is a *direct one* while in the latter phase it is *indirect*.

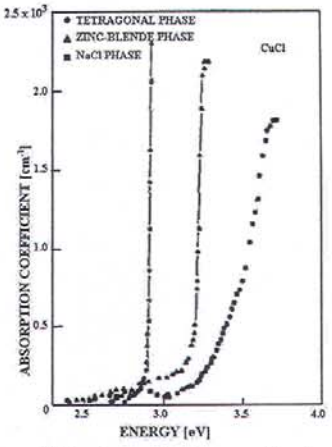

Fig. 18. Plot of the absorption coefficient α against energy for the zinc-blende, tetragonal, and NaCl-type phases at 3.8, 5.8, and 13.2 GPa, respectively.

In Fig. 19 the pressure dependence of the energy gap in CuCl is shown. The decrease at about 4.8 GPa is due to the zinc-blende tetragonal transition. The change near 9 GPa is due to the tetragonal - NaCl-type transition. These results gave clear evidence against the insulator-metal transition reported earlier [28].

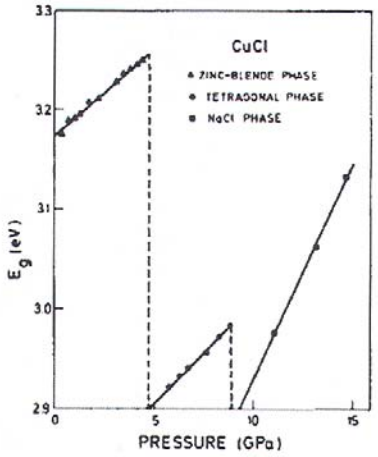

Fig. 19. Pressure dependence of the energy gap in CuCl.

3. 3. Luminescence measurements

The observation of a crossing of crystal field levels in 1% Pr^{3+} in $LaCl_3$

The rare earth halides are interesting due to the fact, that "laser action" has been reported at room temperature in pure $PrCl_3$ [29]. The potentially large gain in such concentrated materials makes it interesting to study the electronic properties, like crystal field splitting, in greater detail. Therefore we have studied the dependence of the ground state splitting of Pr^{3+} in $LaCl_3$ on hydrostatic pressure. Experimental determination of the ground state splitting of the Pr^{3+} ion may easily be accomplished by the investigation of the optical transition from the $^3P_0$ level to the $^3H_4$ ground state multiplet. Since the upper electronic level exhibits no crystal field splitting the fine structure of this transition directly displays the ground state splitting. The nine-fold degenerate electronic ground state $^3H_4$ of Pr^{3+} splits into six crystal field levels under the influence of the crystal field with D_{3h} symmetry. According to symmetry selection rules transitions from $^3P_0$ to the A''_2 and E' levels of $^3H_4$ are allowed. The lowest level E' is followed in energy at normal pressure by the excited A''_2 and E' levels at 34 and 98 cm^{-1}, respectively [29].

Fig. 20 shows the fluorescence spectra of $LaCl_3:Pr^{3+}$ at 25 K and different pressures. The sharpness of the bands is due to the weak electron-phonon coupling of f–electron systems (in contrast to d-electron systems). Despite the pressure induced broadening the bands are very well resolved even at 13.6 GPa. This has allowed us to observe the crossing of crystal field levels at about 11.5 GPa, displayed in Fig. 21. The pressure dependent crystal field splitting can be explained due to the variation of the crystal field with coordination geometry, as discussed in detail in Ref. 30.

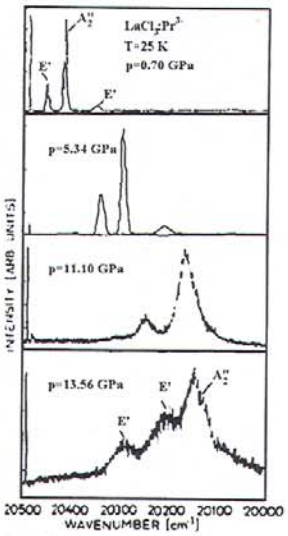

Fig. 20. Fluorescence spectra of $LaCl_3:Pr^{3+}$ at 25 K and different pressures.

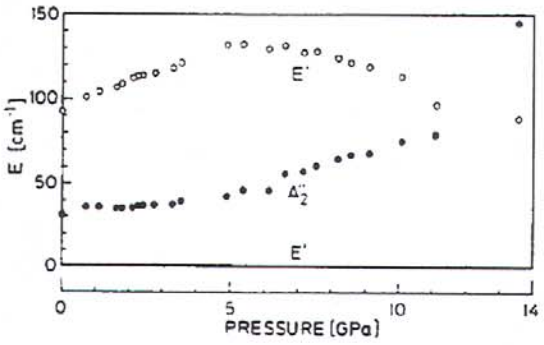

Fig. 21 Relative energy shifts of the crystal field split levels of Pr^{3+} in $LaCl_3:Pr^{3+}$. (The errors are indicated by the diameter of the dots).

3.4. Brillouin scattering

Alkali cyanides

The alkali cyanides display many interesting properties which arise from the molecular character of the CN^- ion. We report here the results of a high pressure Brillouin scattering study of the phase transition in KCN occurring at T_c = 168 K at ambient pressure, in which KCN transforms from a high temperature fcc structure with CN^- directional disorder to a lower temperature orthorhombic structure with directional order but head-to-tail randomness.

Haussühl [31] used 15 MHz ultrasonic measurements to show that C_{44} softens very markedly, tending to zero at a temperature T_0 about 14 K below T_c. He concluded, therefore, that C_{44} was directly involved in the phase transition. In order to check if the phase transition is driven by a soft TA-mode associated with C_{44}, one has to check for dispersion effects and if $\partial T_0/\partial P = \partial T_c/\partial P$. Our high pressure Brillouin study revealed that there are no dispersion effects and that C_{44} and T_0 are independent of pressure (Fig. 22). Therefore, the softening of C_{44} is not the driving mechanism for the phase transition.

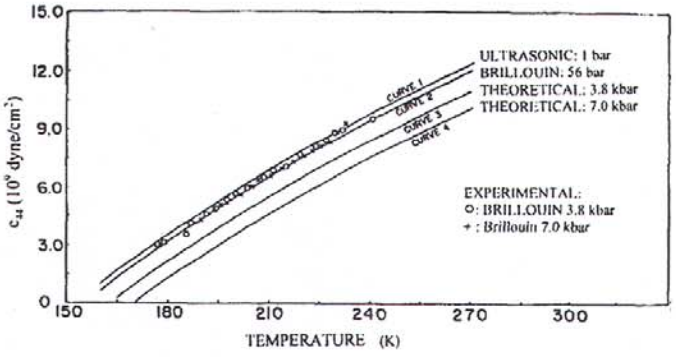

Fig. 22. Isobaric temperature dependence of C_{44}. Theoretical curves, $C_{44} = a \ln|T/(T0)p|$ with $a=21.9 \times 10^9$ dyne/cm^2 and $(T_0)_p=(T_0)_{1bar} + (\partial T_c/\partial P)_T P$. $(T_0)_{1bar}=155.9$ K, $(\partial T_c/\partial P)_T=2$ K/kbar. Curve 1, least square fit to the ultrasonic date of Haussühl [31]; curve 2, least square fit to the values of C_{44} determined from Brillouin shifts at 56 bar.

3.5. Energy-dispersive X-ray diffraction

a) YbO (Valence transition)

YbO has been synthesized under high pressure and it was found to have the expected NaCl-type structure [32]. Its lattice parameter (4.88 Å), black colour, and semiconducting properties indicate that the Yb ion is in the divalent state. This makes YbO a good candidate for a pressure induced valence change. With this expectation we undertook a high pressure X-ray study. The pressure-volume relationship (Fig. 23) clearly indicates abnormal compressibility starting near 8 GPa, strongly suggesting a change in the valence state of Yb towards trivalency. The transition appears to be gradual and, as expected, isostructural. Furthermore, there is a change in the colour of the material from black to golden yellow at high pressure, suggestive of the metallic character which is consistent with the valence change.

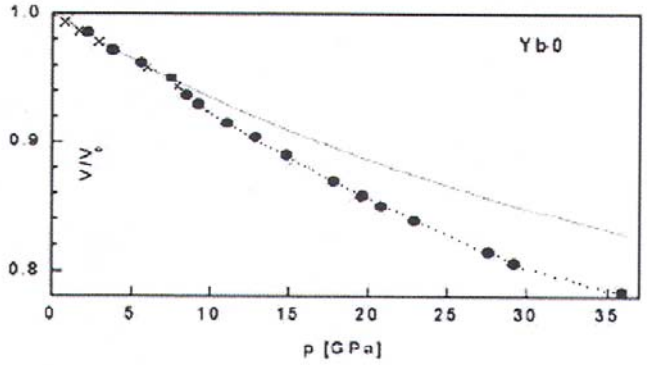

Fig. 23. Pressure-volume relationship for YbO. The solid line was calculated using the Murnaghan equation of state with B_0 = 130 GPa and B'_0 = 4. The experimental points deviate after 8 GPa due to valence change. The experimental conditions are indicated by the following symbols: ×: without pressure medium; ●: with Si - grease as a pressure medium; ■: with 4:1 methanol, methanol mixture as pressure medium.

b) Alkali hydrides

The interest in the alkali hydrides has been generated by their crystallo-chemical similarity to the alkali halides. Bashkin et al. [33] have pointed out, that as in the case of most alkali halides with NaCl-type structure, the alkali hydrides may also undergo a structural phase transition to a CsCl-type structure when high pressure is applied. They have found such a transition in KH at about 4 GPa and have predicted that this transition is thermodynamically possible also in NaH, RbH, and CsH, but not in LiH. We have undertaken a high pressure X-ray study in order to confirm this prediction experimentally. Fig. 24 shows the energy dispersive X-ray pattern of KH in the NaCl-type (2.40 GPa) and CsCl-type structure (6.40 GPa).

Fig. 25 shows the p-V data of KH. In agreement with Bashkin et al. [33], we find the phase transition from the NaCl-type structure at 4.0 GPa. Figs. 26 and 27 show the p–V data of RbH and CsH, respectively. The transition in CsH occurs at 1.2 GPa, whereas in the case of RbH a coexistence region of the NaCl-type and CsCl-type structure exists between 2.2 and 3.1 GPa.

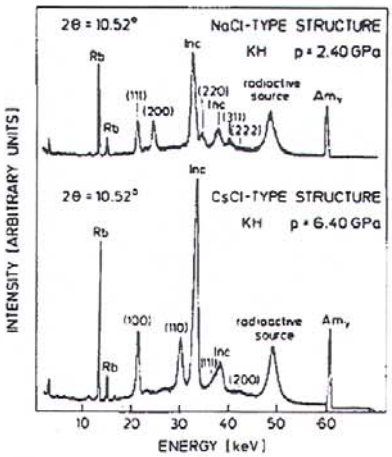

Fig. 24. Energy dispersive X-ray diagram of the NaCl-type and CsCl-type phase of KH. The reflections are labeled by their (hkl)-indices. The additional peaks in the energy dispersive X-ray diagram are caused by reflections from the body-centered Inconel gasket material [(111) strong and (200) weak] and from the radioactive Americium source with the element rubidium as a target. The average value 13.37 keV of the $K\alpha_{1,2}$ radiation of Rb and the Americium γ-radiation (Amλ) at 60.54 keV were used for energy calibration.

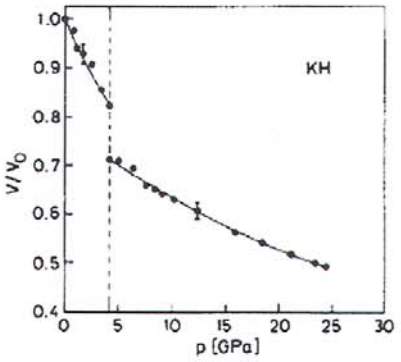

Fig. 25. p-V data of KH. (The full line represents a fit of the Birch equation of state to the data points. The vertical dashed line separates the NaCl - type and CsCl - type phases).

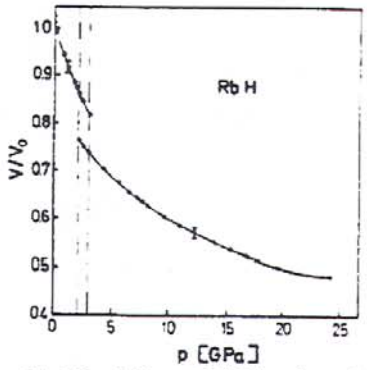

Fig. 26. p-V data of RbH (see legend Fig. 25).

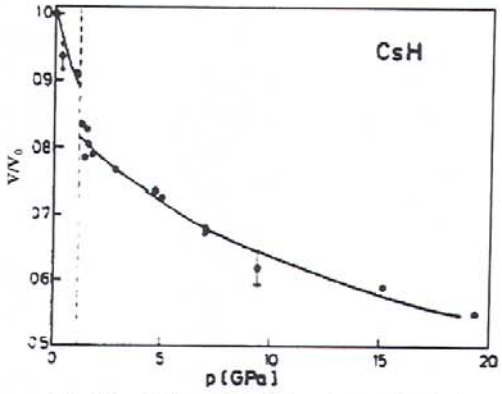

Fig. 27. p-V data of CsH (see legend Fig. 25).

Fig. 28 shows the p-V data for NaH. No transition has been observed up to 28 GPa, the highest pressure of this experiment. Duclos et al. [34] have extended the study of NaH to 54 GPa and found the NaCl-type to CsCl-type transition at 29.3 ± 0.9 GPa.

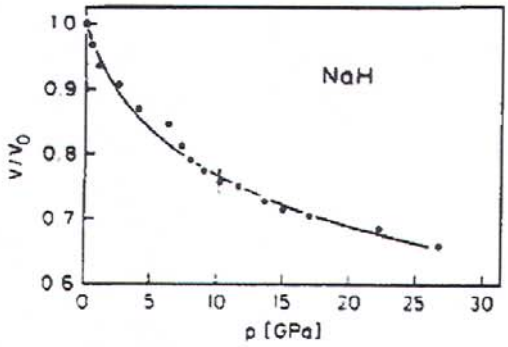

Fig. 28. p-V data of NaH. (The full line represents a fit of the Birch equation of state to the data points).

3. 6. Conductivity measurements

a) Cr rich Cr-Ge alloys

From the pressure dependence of the Néel temperature (TN) of Cr rich Cr-Ge alloys we have shown that the commensurate spin-density wave (CSDW) state becomes stable in alloys with more than 0.6 at. % Ge (Fig. 29). The stabilization of the commensurate phase for Ge addition violates the ratio rule [35]. A detailed discussion of the results can be found in Ref. [36].

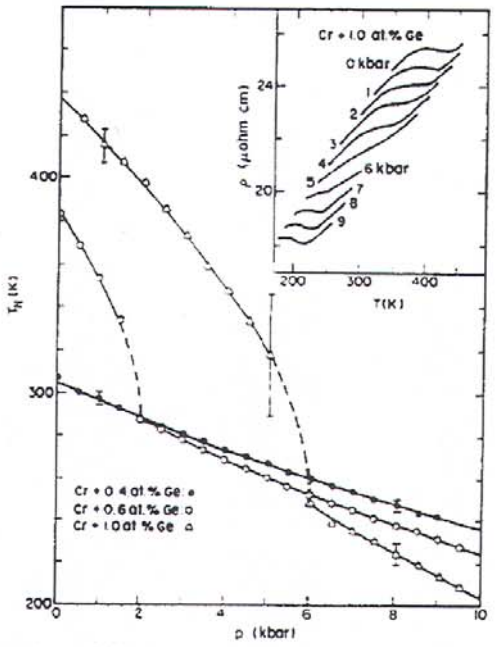

Fig. 29. Pressure dependence of the Néel temperature for Cr-Ge alloys. The solid line has been drawn connecting the data points. The insert shows the resistance anomaly associated with the transition.

4. Conclusions

It has been shown that Raman scattering measurements provide an excellent tool to determine p-T phase diagrams. However, one must have reliable structural data to determine the allowed Raman active modes using group theory. Without this information changes in the features of the Raman spectra can be misinterpreted as an indicator of a phase transition. The example of CuCl shows that a careful study of the pressure dependence of the band gap would have prevented the claim that CuCl will become metallic [37] and superconducting at high pressure [38-40]. The high pressure luminescence measurements on 1% Pr^{3+} in $LaCl^3$ provide for the first time evidence of a crossing of crystal field levels which could be explained by variation of the crystal field with coordination geometry. The high pressure Brillouin study provided evidence that the observed phase transition in KCN is not driven by a soft TA-mode [31]. The softening is due to a rotational-translational coupling, which has the effect of making the eigenvalues of the static susceptibility temperature dependent [41]. Furthermore, the high pressure Brillouin scattering study provided evidence of the importance of anharmonicities which had to be included in the theoretical model to account for the observed softening [42].

The energy dispersive X-ray diffraction studies provided evidence for the metallization of YbO at high pressure. In the case of the alkali hydrides we confirmed the occurrence of a phase transition from the NaCl to the CsCl structure at high pressure. This has been predicted by Bashkin et al. [33] based on the assumption of a similar behaviour of alkali hydrides and alkali halides. The final example of high pressure conductivity measurements on Cr-rich Cr-Ge alloys provided proof that a commensurate phase exists also in this material. It has been claimed that such a phase could not exist in Cr-Ge alloys [43, 44].

Acknowledgements

I would like to acknowledge the contributions of colleagues who have been involved in the different studies presented in this paper. They are listed in alphabetical order: T. Geisel, A. Jayaraman, G. A. Kourouklis, R. Kremer, W. Love, G. Materlik, D. Strauch, K. Strössner, W. Urland, Ch. T. Walker, A. Werner.

References

[1] The Review of High Pressure Science and Technology, **7** (1998); Proceedings of International Conference-AIRAPT-16 and HPCJ-38-on High Pressure Science and Technology, Kyoto, Japan, ed. M. Nakahara, Nakanishi Printing Co.,Ltd., 25-29 August 1997.
[2] P. S. Peercy, B. Morosin, Phys. Rev., **B7**, 2779 (1973).
[3] H. D. Hochheimer, M. L. Shand, J. E. Potts, R. C. Hanson, C. T. Walker, Phys. Rev., **B14**, 4630 (1976).
[4] R. A. Cowley, Philos. Mag., **11**, 673 (1965); Adv. Phys., **12**, 421 (1963).
[5] A. A. Maradudin, A. E. Fein, Phys. Rev., **128**, 2589 (1962).
[6] R. Loudon, Proc. Roy. Soc., **A275**, 218, (1963).
[7] "The Raman Effect" in two Volumes, Vol. **2,** Applications: ed. by A. Anderson, Marcel Dekker, Inc., New York, 1973.
[8] M. Born, M. Bradbury, Proc. Roy. Soc., **A188**, 161 (1947).
[9] G. Will, Fortschr. Miner., **59**, 31 (1981).
[10] J. Bordas, A. M. Glazer, C. J. Howard, A. J. Bourdillon, Phil. Mag., **35**, 311 (1977).
[11] B. Buras, J. Staun Olsen, A. Lindegaard Andersen, L. Gerward, B. Selsmark, Monograph no. 73-12, Physical Laboratory II, H.C. Oerstedt Institute, University of Copenhagen, Universitetsparken 5, DK-2100 Copenhagen, Denmark (1973).
[12] R. J. Hemley, P.M. Bell, H. K. Mao, Science, **237**, 605 (1987).
[13] H. D. Hochheimer, W. F. Love, Ch. T. Walker, Phys. Rev. Letters, **38**, 832 (1977).

[14] W. F. Love, H. D. Hochheimer, M. W. Anderson, R. N. Work, C. T. Walker, Solid State Commun., **23**, 365 (1977).
[15] K. Stroessner, W. Henkel, H. D. Hochheimer, M. Cardona, Solid State Commun., **47**, 567 (1983).
[16] K. Stoessner, H. D. Hochheimer, J. Chem. Phys., **82**, 5364 (1985).
[17] H. D. Hochheimer, K. Weishaupt, M. Takesada, J. Chem. Phys., **105**, 374 (1996).
[18] K. Weishaupt, M. Takesada, A. Simon, M. P. Gelfand, A. Onodera, H. D. Hochheimer, Phys. Rev., **B57**, 5693 (1998).
[19] J. R. Sandercock, Proc. Int. Conference on Light Scattering in Solids, ed. M. Balkanski, Flammarion, p. 9, Paris 1971.
[20] J. R. Sandercock, J. Phys. E, Sci. Instrum., **9**, 566 (1976).
[21] J. R. Sandercock, Solid State Commun., **26**, 547 (1978).
[22] Ch. H. Whitfield, E. M. Brody, Rev. Sci. Instrum., **47**, 942 (1976).
[23] R. Stevenson, J. Chem. Phys., **34**, 1757 (1961).
[24] S. A. Zlunitsyn, Zh. Eksp. Teor. Fiz., **8**, 724 (1938); **9**, 72 (1939); cited in Ref. 18.
[25] H. D. Hochheimer, E. Spanner, D. Strauch, J. Chem. Phys., **64**, 1583 (1976).
[26] H. D. Hochheimer, T. Geisel, J. Chem. Phys., **64**, 1586 (1976).
[27] D. Müller, H. Hahn, Z. Anorg. Allg. Chem., **438**, 258 (1978).
[28] C. W. Chu, A. P. Rusakov, S. Huang, S. Early, T. H. Geballe, C. Y. Huang, Phys. Rev., **B18**, 2116 (1978).
[29] C. F. Varsanyi, Appl. Phys. Lett., **19**, 169 (1971).
[30] W. Urland, H. D. Hochheimer, G. A. Kourouklis, R. Kremer, Solid State Commun., **13,** 649 (1985.
[31] S. Haussühl, Solid State Commun., **13**, 147 (1973).
[32] J. M. Leger, N. Yacoubi, J. Loriers, in "The Rare Earths in Modern Science and Technology", ed. G. J. McCarthy, J. J. Rhynne, H. B. Silber, Vol. **2**, Plenum Press, New York and London, p. 203, 1979.
[33] I. O. Bashkin, T. N. Dymova, E. G. Ponyatovskii, phys. stat. sol. (b), **100**, 87 (1980).
[34]. S. J. Duclos, Y. K. Vohra, A. L. Ruoff, S. Filipek, B. Baranowski, Phys. Rev., **B36**, 7664 (1987).
[35] T. M. Rice, A. Jayaraman, D. B. McWhan, J. Phys. (Paris), Colloq., **32**, C1 (1971).
[36] H. D. Hochheimer, R. Münch, Phil. Mag., **B63**, 979 (1991).
[37] C. W. Chu, S. Early, T.H. Geballe, A. Rusakov, R. E. Schwall, J. Phys. C: Sol. State Phys., **8**, L241 (1975).
[38] A. P. Rusakov, phys. stat. sol. (b), **72**, 503 (1975).
[39] A. P. Rusakov, High Temp.-High Pressures, **8**, 662 (1976).
[40] N. B. Brandt, S. V. Kuvshinnikov, A. P. Rusakov, M. V. Semenov, JETP Letters, **27**, 37 (1978).
[41] K. H. Michel, J. Naudts, Phys. Rev. Lett., **39**, 212 (1977); J. Chem. Phys., **65**, 977 (1976).
[42] J. Naudts, K. H. Michel, Phys. Rev., **B18**, 667 (1978).
[43] S. Arajs, W. E. Katzenmeyer, J. Phys. Chem. Solids, **28**, 1459 (1967).
[44] P. A. Fedders, P. C. Martin, Phys. Rev., **143**, 245 (1966).